AIMS Mathematics, 10(9): 20235–20261.
DOI:10.3934/math.2025904
Received: 13 July 2025
Revised: 17 August 2025
Accepted: 26 August 2025
Published: 04 September 2025

https://www.aimspress.com/journal/Math

Research article

Mathematical and numerical analysis of a fractional SIQR epidemic model with normalized Caputo–Fabrizio operator and machine learning approaches

Ramsha Shafqat[1,*] **and Ateq Alsaadi**[2]

[1] Department of Mathematics and Statistics, The University of Lahore, Sargodha 40100, Pakistan
[2] Department of Mathematics and Statistics, College of Science, Taif University, P. O. Box 11099, Taif 21944, Saudi Arabia

* **Correspondence:** Email: ramshawarriach@gmail.com.

Abstract: This paper introduces, analyzes, and numerically investigates a fractional-order SIQR epidemic model with the normalized Caputo–Fabrizio derivative. The model captures memory effects and the impact of quarantine or isolation interventions, offering a more realistic description of epidemic dynamics. We establish the existence, uniqueness, positivity, and population conservation properties, and then propose a robust numerical scheme. The influence of the memory parameter and kernel normalization is illustrated via simulations, with a discussion on their implications for epidemic forecasting and real-world control strategies. Furthermore, artificial neural networks are applied, with the dataset partitioned into training, validation, and testing subsets. A comprehensive assessment is carried out for each dataset partition.

Keywords: fractional differential equation; normalized Caputo–Fabrizio; SIQR model; numerical outcomes; machine learning
Mathematics Subject Classification: 34D20, 34K20, 34K60, 92C60, 92D45

1. Introduction

Mathematical modeling is a cornerstone for analyzing, predicting, and managing the transmission dynamics of infectious diseases [1, 2]. Among various frameworks, compartmental models, such as the susceptible-infectious-recovered (SIR) model and its extensions, are fundamental tools for capturing epidemic spread and informing public health interventions [3]. However, classical integer-order models often fail to account for the memory and hereditary properties present in real epidemics, such as variable infectious periods, delayed effects of control measures, and non-exponential waiting times [4, 5].

Fractional-order differential equations have thus gained prominence in epidemiological modeling for their ability to incorporate memory effects, whereby the system's current state depends on its historical trajectory [5–7]. The Caputo derivative, with its power-law kernel, is widely used but suffers from singularities, while the Caputo–Fabrizio (CF) derivative, featuring a non-singular exponential kernel, offers both computational advantages and physically realistic fading memory [8–10]. Nonetheless, the standard CF kernel is not normalized, which can introduce inconsistencies in the interpretation and scaling of memory effects. The normalized Caputo-Fabrizio (NCF) derivative addresses this limitation by ensuring the kernel integrates to unity, thereby preserving the operator's interpretation as a true weighted average [11].

In recent years, significant progress has been made in the study of control and synchronization of nonlinear and fractional-order systems. For instance, Zhang et al. [12] proposed a dynamic event-based tracking control strategy for boiler turbine systems, ensuring guaranteed performance and contributing to practical engineering applications. You and Zhang [13] developed a finite-time synchronization method for fractional-order chaotic systems based on the maximum-valued method of functions of five variables. Moreover, Kao et al. [14] investigated projective synchronization for uncertain fractional reaction-diffusion systems through an adaptive sliding mode control scheme with a finite-time guarantee, while Kao et al. [15] further explored Mittag–Leffler synchronization of delayed fractional memristor neural networks via adaptive control. Complementarily, Cao et al. [16] analyzed the global Mittag–Leffler stability of delayed fractional coupled reaction-diffusion systems on networks without strong connectivity. Extending this line of research, Cao et al. [17] introduced a sliding mode control framework for uncertain fractional-order reaction-diffusion memristor neural networks with time delays. Additionally, Kao et al. [18] investigated global Mittag–Leffler synchronization of coupled delayed fractional reaction-diffusion Cohen–Grossberg neural networks using sliding mode control. These works collectively highlight the growing importance of advanced control and synchronization methods in both theoretical research and engineering systems.

Despite theoretical and practical advances, fractional epidemic models employing quarantine or isolation strategies have not been systematically explored with the NCF derivative. The SIQR model enhances the classical SIR framework by incorporating a quarantined class, which captures the impact of interventions such as quarantine, isolation, or hospitalization, playing a critical role in disease control (e.g., COVID-19, SARS, Ebola).

This study presents, analyzes, and numerically investigates a fractional SIQR epidemic model governed by the NCF operator. We provide a rigorous mathematical analysis of the model's properties (existence, uniqueness, positivity, and boundedness), derive a robust numerical scheme, and compare the NCF-SIQR model with its classical and unnormalized fractional counterparts.

In addition to classical numerical analysis, we leverage artificial neural networks (ANNs) to approximate the compartmental solutions and perform model validation. Recent research demonstrates that machine learning and deep learning algorithms can effectively complement fractional-order models, offering improved predictive accuracy, noise tolerance, and the ability to learn complex patterns from simulation or empirical data [19–21]. In our approach, ANN techniques are used to fit and predict the solution trajectories of the SIQR compartments as shown in Figure 1, with performance evaluated using mean squared error, regression analysis, and error distribution metrics.

The primary objectives of this work are as follows:

- Develop and analyze a fractional SIQR epidemic model using the NCF derivative.

- Prove the essential mathematical properties of the model.
- Propose and implement a reliable numerical scheme.
- Demonstrate the effectiveness of both numerical and ANN-based approaches through comprehensive simulations and comparative analyses.

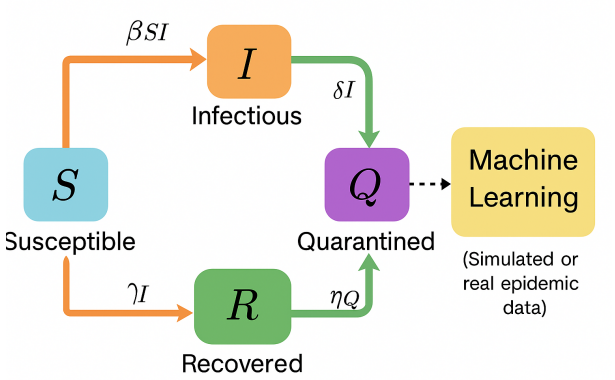

Figure 1. Schematic diagram of the SIQR model.

Section 2 reviews the necessary preliminaries on fractional derivatives and machine learning concepts. Section 3 presents the model formulation. Section 4 details the theoretical analysis. Section 5 introduces the numerical method. Section 6 reports the simulation and ANN results. Section 7 provides concluding remarks and outlines directions for future research.

2. Preliminaries

Before proceeding, we present the following definitions, which will be fundamental in the development of our main results.

Definition 2.1. *[22] For* $0 < \alpha < 1$*, the CF derivative of a function* $u(t)$ *is*

$$({}^{CF}D_0^{\alpha}u)(t) = \frac{1}{1-\alpha}\int_0^t e^{-\mu_\alpha(t-s)}u'(s)ds,$$

where $\mu_\alpha = \frac{\alpha}{1-\alpha}$.

Definition 2.2. *[23] The NCF derivative is defined by*

$$({}^{NCF}D_0^{\alpha}u)(t) = \frac{1}{(1-\alpha)C_\alpha(t)}\int_0^t e^{-\mu_\alpha(t-s)}u'(s)ds,$$

where

$$C_\alpha(t) = \frac{1}{\alpha}(1-e^{-\mu_\alpha t}).$$

This normalization ensures the kernel integrates to 1 over $[0, t]$.

3. Model formulation

We consider the normalized fractional SIQR model:

$$\begin{aligned} ({}^{NCF}D_0^{\alpha}S)(t) &= -\beta S(t)I(t), \\ ({}^{NCF}D_0^{\alpha}I)(t) &= \beta S(t)I(t) - (\gamma+\delta)I(t), \\ ({}^{NCF}D_0^{\alpha}Q)(t) &= \delta I(t) - \eta Q(t), \\ ({}^{NCF}D_0^{\alpha}R)(t) &= \gamma I(t) + \eta Q(t), \\ S(0) = S_0 \geq 0, I(0) = I_0 \geq 0, &Q(0) = Q_0 \geq 0, R(0) = R_0 \geq 0, \end{aligned} \tag{3.1}$$

where β is the infection rate, γ is the recovery rate from the infectious class, δ is the isolation (quarantine) rate, and η is the recovery rate from the quarantined class. The total initial population is $N_0 = S_0 + I_0 + Q_0 + R_0$.

In this framework, the functions $S(t)$, $I(t)$, $Q(t)$, and $R(t)$ represent the proportions of the population that are susceptible, infectious, quarantined (isolated), and recovered at any time t, respectively. The operator ${}^{NCF}D_0^{\alpha}$ denotes the NCF fractional derivative of order $\alpha \in (0, 1)$. This fractional derivative introduces memory effects into the system via a normalized, non-singular kernel, allowing the model to reflect how previous states influence current epidemic dynamics.

The first equation models the depletion of susceptible individuals due to infection. The second equation captures the growth of infectious individuals by new infections and their removal via recovery and isolation. The third equation describes the flow into and out of the quarantined compartment, governed by the isolation and quarantine recovery rates. The fourth equation tracks the accumulation of recovered individuals from both infectious and quarantined classes. The initial conditions S_0, I_0, Q_0, and R_0 set the initial state of the population, with all compartments assumed non-negative and summing to N_0.

By extending the classical SIR model to incorporate quarantine and memory effects through the NCF derivative, this formulation enables the modeling of key control interventions and the retention of epidemic memory, including the impact of past exposures, the effectiveness of isolation, and changing recovery rates. As $\alpha \to 1$, the NCF-SIQR model recovers the classical SIQR model with integer-order derivatives. The use of a normalized kernel ensures the overall memory contribution is well-scaled. It avoids the mathematical singularities of classical fractional operators, thereby improving the model's ability to capture and predict realistic epidemic processes involving quarantine and isolation.

4. Comparison to classical and Caputo–Fabrizio Models

This section provides a comparative overview of the standard SIQR model, its Caputo fractional formulation, the CF version, and the NCF-SIQR model (see Table 1).

Table 1. Comparison of different SIQR models.

Model	Kernel type	Advantages	Disadvantages	Application notes
Classical SIQR	Integer-order derivative	Simple formulation; well-understood theory; fast computation	Cannot capture memory effects or non-exponential waiting times	Suitable for short-term outbreaks with negligible historical dependence
Caputo Fractional SIQR	Power-law kernel (singular)	Captures long-memory effects; flexible modeling	kernel singularity causes computational challenges; interpretation less intuitive	Useful for diseases with strong long-term memory in dynamics
CF Fractional SIQR	Non-singular exponential kernel	Avoids kernel singularity; computationally efficient	kernel not normalized scaling of memory effects can be inconsistent	Appropriate for modeling fading memory without singularity issues
NCF Fractional SIQR (Proposed)	Non-singular exponential kernel with normalization	Retains computational efficiency; normalized kernel ensures consistent scaling and interpretability; physically realistic memory weighting	Slightly higher computation than unnormalized CF	Ideal for epidemic modeling with fading memory and intervention effects such as quarantine

4.1. Classical SIQR model

The classical SIQR model with integer-order derivatives is:

$$\begin{aligned}
\frac{dS}{dt} &= -\beta S I, \\
\frac{dI}{dt} &= \beta S I - (\gamma + \delta) I, \\
\frac{dQ}{dt} &= \delta I - \eta Q, \\
\frac{dR}{dt} &= \gamma I + \eta Q,
\end{aligned}$$

where $S(t)$, $I(t)$, $Q(t)$, and $R(t)$ denote the susceptible, infectious, quarantined, and recovered compartments, respectively. Here, β is the infection rate, γ is the recovery rate from the infectious class, δ is the isolation (quarantine) rate, and η is the recovery rate from the quarantined class.

4.2. Caputo fractional SIQR model

The Caputo fractional SIQR model replaces the integer-order derivatives with Caputo fractional derivatives ($0 < \alpha < 1$):

$$\begin{aligned} {}^{C}D_0^{\alpha} S(t) &= -\beta S(t) I(t), \\ {}^{C}D_0^{\alpha} I(t) &= \beta S(t) I(t) - (\gamma + \delta) I(t), \\ {}^{C}D_0^{\alpha} Q(t) &= \delta I(t) - \eta Q(t), \\ {}^{C}D_0^{\alpha} R(t) &= \gamma I(t) + \eta Q(t), \end{aligned}$$

where the Caputo derivative [24] is defined as

$${}^{C}D_0^{\alpha} u(t) = \frac{1}{\Gamma(1-\alpha)} \int_0^t (t-s)^{-\alpha} u'(s)\, ds.$$

4.3. Caputo–Fabrizio fractional SIQR model

The CF-SIQR model uses the CF fractional derivative:

$$\begin{aligned} ({}^{CF}D_0^{\alpha} S)(t) &= -\beta S(t) I(t), \\ ({}^{CF}D_0^{\alpha} I)(t) &= \beta S(t) I(t) - (\gamma + \delta) I(t), \\ ({}^{CF}D_0^{\alpha} Q)(t) &= \delta I(t) - \eta Q(t), \\ ({}^{CF}D_0^{\alpha} R)(t) &= \gamma I(t) + \eta Q(t), \end{aligned}$$

where

$$({}^{CF}D_0^{\alpha} u)(t) = \frac{1}{1-\alpha} \int_0^t e^{-\mu_\alpha (t-s)} u'(s)\, ds, \qquad \mu_\alpha = \frac{\alpha}{1-\alpha}.$$

4.4. Normalized Caputo–Fabrizio SIQR model

The NCF-SIQR model is given by:

$$\begin{aligned} ({}^{NCF}D_0^{\alpha} S)(t) &= -\beta S(t) I(t), \\ ({}^{NCF}D_0^{\alpha} I)(t) &= \beta S(t) I(t) - (\gamma + \delta) I(t), \\ ({}^{NCF}D_0^{\alpha} Q)(t) &= \delta I(t) - \eta Q(t), \\ ({}^{NCF}D_0^{\alpha} R)(t) &= \gamma I(t) + \eta Q(t), \end{aligned}$$

where

$$({}^{NCF}D_0^{\alpha} u)(t) = \frac{1}{(1-\alpha) C_\alpha(t)} \int_0^t e^{-\mu_\alpha (t-s)} u'(s)\, ds, \quad C_\alpha(t) = \frac{1}{\alpha}(1 - e^{-\mu_\alpha t}).$$

5. Theoretical analysis

We establish the existence and uniqueness of solutions to the NCF-SIQR system, thereby providing a foundation for the mathematical validity of the model. The demonstration relies on fixed-point theory and essential characteristics of the NCF fractional operator.

5.1. Existence and uniqueness of solutions

Before analyzing the dynamics, we establish that the NCF-SIQR model admits a unique global solution. This guarantees the mathematical consistency and reliability of the system.

Theorem 1. *There exists a unique global solution* (S, I, Q, R) *to the NCF-SIQR system on the interval* $[0, T]$.

Proof. We rewrite the NCF-SIQR model using properties of the NCF operator (see [9]):

$$\begin{aligned}
S(t) &= S_0 + (1-\alpha)C_\alpha(t)\left[-\beta S(t)I(t)\right] + \alpha\int_0^t C_\alpha(\tau)\left[-\beta S(\tau)I(\tau)\right]d\tau,\\
I(t) &= I_0 + (1-\alpha)C_\alpha(t)\left[\beta S(t)I(t) - (\gamma+\delta)I(t)\right] + \alpha\int_0^t C_\alpha(\tau)\left[\beta S(\tau)I(\tau) - (\gamma+\delta)I(\tau)\right]d\tau,\\
Q(t) &= Q_0 + (1-\alpha)C_\alpha(t)\left[\delta I(t) - \eta Q(t)\right] + \alpha\int_0^t C_\alpha(\tau)\left[\delta I(\tau) - \eta Q(\tau)\right]d\tau,\\
R(t) &= R_0 + (1-\alpha)C_\alpha(t)\left[\gamma I(t) + \eta Q(t)\right] + \alpha\int_0^t C_\alpha(\tau)\left[\gamma I(\tau) + \eta Q(\tau)\right]d\tau,
\end{aligned}$$

where $C_\alpha(t)$ is the normalization function of the kernel.

Let $X = [C([0, T])]^4$, the Banach space of continuous vector-valued functions on $[0, T]$ with norm

$$\|U\| = \max\{\|S\|_\infty, \|I\|_\infty, \|Q\|_\infty, \|R\|_\infty\}.$$

Define the nonlinearities as

$$\begin{aligned}
f_1 &= -\beta S I,\\
f_2 &= \beta S I - (\gamma+\delta)I,\\
f_3 &= \delta I - \eta Q,\\
f_4 &= \gamma I + \eta Q.
\end{aligned}$$

Define the operator $\mathcal{T}$ on X by:

$$\mathcal{T}\begin{pmatrix} S\\ I\\ Q\\ R\end{pmatrix}(t) = \begin{pmatrix}
S_0 + (1-\alpha)C_\alpha(t)f_1(S(t), I(t), Q(t), R(t)) + \alpha\int_0^t C_\alpha(\tau)f_1(S(\tau), I(\tau), Q(\tau), R(\tau))\,d\tau\\
I_0 + (1-\alpha)C_\alpha(t)f_2(S(t), I(t), Q(t), R(t)) + \alpha\int_0^t C_\alpha(\tau)f_2(S(\tau), I(\tau), Q(\tau), R(\tau))\,d\tau\\
Q_0 + (1-\alpha)C_\alpha(t)f_3(S(t), I(t), Q(t), R(t)) + \alpha\int_0^t C_\alpha(\tau)f_3(S(\tau), I(\tau), Q(\tau), R(\tau))\,d\tau\\
R_0 + (1-\alpha)C_\alpha(t)f_4(S(t), I(t), Q(t), R(t)) + \alpha\int_0^t C_\alpha(\tau)f_4(S(\tau), I(\tau), Q(\tau), R(\tau))\,d\tau
\end{pmatrix}$$

We will show $\mathcal{T}$ is a contraction on a suitable subset of X by proving each f_j is Lipschitz continuous on bounded sets. Let $D_M = \{(S, I, Q, R) \in X : \|S\|, \|I\|, \|Q\|, \|R\| \le M\}$ for some $M > 0$.

For all $(S_1, I_1, Q_1, R_1), (S_2, I_2, Q_2, R_2)$ in D_M:

$$\begin{aligned}
|f_1(S_1, I_1, Q_1, R_1) - f_1(S_2, I_2, Q_2, R_2)| &= |-\beta S_1 I_1 + \beta S_2 I_2|\\
&= \beta|S_2 I_2 - S_1 I_1|\\
&= \beta|S_2(I_2 - I_1) + (S_2 - S_1)I_1|\\
&\le \beta(|S_2||I_2 - I_1| + |I_1||S_2 - S_1|)\\
&\le 2\beta M\|(S_1, I_1, Q_1, R_1) - (S_2, I_2, Q_2, R_2)\|,
\end{aligned}$$

$$
\begin{aligned}
|f_2(S_1, I_1, Q_1, R_1) - f_2(S_2, I_2, Q_2, R_2)| &= |\beta S_1 I_1 - (\gamma + \delta) I_1 - [\beta S_2 I_2 - (\gamma + \delta) I_2]| \\
&= |\beta(S_1 I_1 - S_2 I_2) - (\gamma + \delta)(I_1 - I_2)| \\
&\leq \beta(|S_1||I_1 - I_2| + |I_2||S_1 - S_2|) + (\gamma + \delta)|I_1 - I_2| \\
&\leq (2\beta M + \gamma + \delta)\|(S_1, I_1, Q_1, R_1) - (S_2, I_2, Q_2, R_2)\|
\end{aligned}
$$

$$
\begin{aligned}
|f_3(S_1, I_1, Q_1, R_1) - f_3(S_2, I_2, Q_2, R_2)| &= |\delta I_1 - \eta Q_1 - [\delta I_2 - \eta Q_2]| \\
&= |\delta(I_1 - I_2) - \eta(Q_1 - Q_2)| \\
&\leq \delta|I_1 - I_2| + \eta|Q_1 - Q_2| \\
&\leq (\delta + \eta)\|(S_1, I_1, Q_1, R_1) - (S_2, I_2, Q_2, R_2)\|,
\end{aligned}
$$

$$
\begin{aligned}
|f_4(S_1, I_1, Q_1, R_1) - f_4(S_2, I_2, Q_2, R_2)| &= |\gamma I_1 + \eta Q_1 - \gamma I_2 - \eta Q_2| \\
&= \gamma|I_1 - I_2| + \eta|Q_1 - Q_2| \\
&\leq (\gamma + \eta)\|(S_1, I_1, Q_1, R_1) - (S_2, I_2, Q_2, R_2)\|.
\end{aligned}
$$

Let L_M be the largest of the coefficients above. For any $U_1, U_2 \in D_M$,

$$\|\mathcal{T}(U_1) - \mathcal{T}(U_2)\| \leq K L_M \|U_1 - U_2\|,$$

where K depends on T, α, and the kernel normalization. By choosing T sufficiently small so that $KL_M < 1$, $\mathcal{T}$ is a contraction on D_M. By Banach's fixed-point theorem, there is a unique fixed point (solution) in D_M on $[0, T_0]$ for some $T_0 > 0$. Since the solutions remain non-negative and bounded by the total population (which is conserved in SIQR models), the local solution can be extended step by step to the whole interval $[0, T]$. □

5.2. Positivity of solutions

Before proceeding, it is essential to verify that the solutions of the NCF-SIQR model remain non-negative for all time, as required by the biological interpretation of the compartments.

Theorem 2. *If $S_0, I_0, Q_0, R_0 \geq 0$, then, $S(t), I(t), Q(t), R(t) \geq 0$ for all $t \geq 0$.*

Proof. Suppose, for contradiction, that there exists a first time $t^* > 0$ such that one of the compartments becomes negative after being nonnegative for all $t < t^*$.
At t^* the system satisfies:

$$
\begin{aligned}
{}^{NCF}D_t S(t) &= -\beta S(t) I(t), \\
{}^{NCF}D_t I(t) &= \beta S(t) I(t) - (\gamma + \delta) I(t), \\
{}^{NCF}D_t Q(t) &= \delta I(t) - \eta Q(t), \\
{}^{NCF}D_t R(t) &= \gamma I(t) + \eta Q(t).
\end{aligned}
$$

If $S(t^*) = 0$ or $I(t^*) = 0$, the corresponding derivative is 0; if $Q(t^*) = 0$, the derivative is $\delta I(t^*) \geq 0$; and if $R(t^*) = 0$, the derivative is $\gamma I(t^*) + \eta Q(t^*) \geq 0$. In all cases, the derivative is nonnegative, preventing the variables from crossing below zero.
This contradicts the assumption of negativity at t^*. Hence, $S(t), I(t), Q(t), R(t) \geq 0$ for all $t \geq 0$. □

5.3. Boundedness (population conservation)

It is essential to ensure that the total population remains bounded and conserved over time. We establish that the sum of all compartments in the NCF-SIQR model does not exceed the initial population.

Theorem 3. *Let $N(t) = S(t) + I(t) + Q(t) + R(t)$. Then, $N(t) = N_0$ for all $t \geq 0$.*

Proof. Add the four equations of the NCF-SIQR system:

$$({}^{NCF}D_0^{\alpha}S) + ({}^{NCF}D_0^{\alpha}I) + ({}^{NCF}D_0^{\alpha}Q) + ({}^{NCF}D_0^{\alpha}R) = 0.$$

By linearity of the NCF derivative,

$$({}^{NCF}D_0^{\alpha}N)(t) = 0.$$

The only solution with $N(0) = N_0$ is $N(t) = N_0$ for all t. By positivity, all variables remain bounded above by N_0. □

5.4. Equilibria and disease-free invariance

Setting all derivatives to zero in the NCF-SIQR model, the equilibrium satisfies $I^* = 0$ and $Q^* = 0$, with $S^* + R^* = N_0$. Thus, the only equilibrium is the disease-free state, $(S^*, I^*, Q^*, R^*) = (S_0^*, 0, 0, R_0^*)$, where $S_0^* + R_0^* = N_0$.

Suppose the initial conditions satisfy $I_0 = 0$ and $Q_0 = 0$. In that case, all solutions remain disease-free for all time, as the right-hand sides of the equations prevent the generation of new infections in the absence of initially infectious or quarantined individuals.

5.5. Stability of the disease-free equilibrium

Next, we examine the stability of the disease-free equilibrium (DFE) to determine the conditions under which the infection dies out in the NCF-SIQR model.

Theorem 4. *The disease-free equilibrium $(S^*, I^*, Q^*, R^*) = (N_0, 0, 0, 0)$ of the NCF-SIQR model is locally asymptotically stable if $\mathcal{R}_0 = \frac{\beta N_0}{\gamma+\delta} < 1$, and unstable if $\mathcal{R}_0 > 1$.*

Proof. Consider the general NCF-SIQR model:

$$\begin{aligned}
({}^{NCF}D_0^{\alpha}S)(t) &= -\beta S(t)I(t),\\
({}^{NCF}D_0^{\alpha}I)(t) &= \beta S(t)I(t) - (\gamma+\delta)I(t),\\
({}^{NCF}D_0^{\alpha}Q)(t) &= \delta I(t) - \eta Q(t),\\
({}^{NCF}D_0^{\alpha}R)(t) &= \gamma I(t) + \eta Q(t),
\end{aligned}$$

where δ is the rate of quarantine and η is the recovery rate from quarantine.

The DFE is $(S^*, I^*, Q^*, R^*) = (N_0, 0, 0, 0)$.

Consider small perturbations near the DFE:

$$S(t) = N_0 + s(t), \quad I(t) = 0 + i(t), \quad Q(t) = 0 + q(t), \quad R(t) = 0 + r(t),$$

where $|s(t)|, |i(t)|, |q(t)|, |r(t)|$ are small.

Linearizing around the DFE and neglecting higher-order terms:

$$
\begin{aligned}
({}^{NCF}D_0^{\alpha} s)(t) &= -\beta N_0 i(t),\\
({}^{NCF}D_0^{\alpha} i)(t) &= \beta N_0 i(t) - (\gamma+\delta) i(t),\\
({}^{NCF}D_0^{\alpha} q)(t) &= \delta i(t) - \eta q(t),\\
({}^{NCF}D_0^{\alpha} r)(t) &= \gamma i(t) + \eta q(t).
\end{aligned}
$$

The subsystem that governs the dynamics of infection is:

$$({}^{NCF}D_0^{\alpha} i)(t) = [\beta N_0 - (\gamma+\delta)] i(t).$$

The corresponding characteristic equation for the linearized system is:

$$\lambda = \beta N_0 - (\gamma+\delta).$$

For the fractional system, the DFE is locally asymptotically stable if the fundamental part of λ is negative, i.e.,

$$\beta N_0 - (\gamma+\delta) < 0 \implies \mathcal{R}_0 = \frac{\beta N_0}{\gamma+\delta} < 1.$$

Thus:

- If $\mathcal{R}_0 < 1$, all solutions decay to zero and the DFE is locally asymptotically stable.
- If $\mathcal{R}_0 > 1$, at least one mode grows, and the DFE is unstable.

□

6. Numerical method

Let $T > 0$ be the final simulation time and $N \in \mathbb{N}$ the total number of time steps. Define a uniform time grid with step size $h = T/N$ and $t_n = nh$, $n = 0, 1, \ldots, N$.

6.1. Discretization of the NCF derivative

The NCF derivative at t_n is approximated by

$$({}^{NCF}D_0^{\alpha} u)(t_n) \approx \frac{1}{(1-\alpha)C_{\alpha}(t_n)} \sum_{k=0}^{n-1} e^{-\mu_{\alpha}(t_n - t_k)} [u_{k+1} - u_k],$$

where $C_{\alpha}(t_n) = \frac{1}{\alpha}(1 - e^{-\mu_{\alpha} t_n})$ and $\mu_{\alpha} = \frac{\alpha}{1-\alpha}$.

6.2. Numerical scheme for the SIQR model

For each variable $u \in \{S, I, Q, R\}$, the update at t_n is given by

$$u_n = u_0 + \frac{1}{(1-\alpha)C_{\alpha}(t_n)} \sum_{k=0}^{n-1} e^{-\mu_{\alpha}(t_n - t_k)} [u_{k+1} - u_k],$$

where u_0 is the initial value. The right-hand sides at each step depend on the current values of S, I, Q, and R.

Step-by-step implementation:

1) **Initialization:** Set S_0, I_0, Q_0, R_0, and model parameters β, γ, δ, η, α. Compute μ_α.
2) **Time stepping:** For $n = 1$ to N:
   (a) Compute $C_\alpha(t_n) = \frac{1}{\alpha}(1 - e^{-\mu_\alpha t_n})$.
   (b) For each $k = 0$ to $n - 1$, calculate the kernel $e^{-\mu_\alpha(t_n - t_k)}$.
   (c) Evaluate increments:

$$\begin{aligned} S_{k+1} - S_k &= -h\beta S_k I_k, \\ I_{k+1} - I_k &= h[\beta S_k I_k - (\gamma + \delta) I_k], \\ Q_{k+1} - Q_k &= h[\delta I_k - \eta Q_k], \\ R_{k+1} - R_k &= h[\gamma I_k + \eta Q_k]. \end{aligned}$$

   (d) Compute the sums:

$$\begin{aligned} \text{sumS} &= \sum_{k=0}^{n-1} e^{-\mu_\alpha(t_n - t_k)}[S_{k+1} - S_k], \\ \text{sumI} &= \sum_{k=0}^{n-1} e^{-\mu_\alpha(t_n - t_k)}[I_{k+1} - I_k], \\ \text{sumQ} &= \sum_{k=0}^{n-1} e^{-\mu_\alpha(t_n - t_k)}[Q_{k+1} - Q_k], \\ \text{sumR} &= \sum_{k=0}^{n-1} e^{-\mu_\alpha(t_n - t_k)}[R_{k+1} - R_k]. \end{aligned}$$

   (e) Update:

$$\begin{aligned} S_n &= S_0 + \frac{1}{(1-\alpha)C_\alpha(t_n)}\text{sumS}, \\ I_n &= I_0 + \frac{1}{(1-\alpha)C_\alpha(t_n)}\text{sumI}, \\ Q_n &= Q_0 + \frac{1}{(1-\alpha)C_\alpha(t_n)}\text{sumQ}, \\ R_n &= R_0 + \frac{1}{(1-\alpha)C_\alpha(t_n)}\text{sumR}. \end{aligned}$$

3) **Repeat** until $n = N$.

6.3. Consistency and accuracy

The proposed numerical method for solving the NCF-SIQR system utilizes the rectangle (left-point) rule to approximate the convolution integral present in the NCF fractional derivative, thereby achieving first-order accuracy in time. As the time step $h \to 0$, the discrete sum converges to the continuous integral, ensuring the consistency of the scheme for all compartments of the model. For higher accuracy, the trapezoidal rule can be employed, yielding a second-order method. Notably, in the classical limit as $\alpha \to 1$, the normalization factor $C_\alpha(t_n)$ approaches t_n, the memory kernel vanishes for earlier steps, and the method reduces to the explicit Euler scheme for the standard SIQR model. While decreasing the time step h improves the numerical accuracy for the variables S, I, Q, and R, it

also increases the computational cost, since the memory term requires summing over all previous steps to account for history-dependent effects.

6.4. Comparison with standard Caputo and Caputo–Fabrizio methods

To understand the impact of kernel normalization, one can also simulate:

- The SIQR model with the standard Caputo derivative (power-law kernel):

$$ {}^{C}D_0^{\alpha} u(t_n) \approx \frac{1}{\Gamma(1-\alpha)} \sum_{k=0}^{n-1} (t_n - t_k)^{-\alpha} [u_{k+1} - u_k], $$

  where u stands for S, I, Q, or R.
- The unnormalized CF SIQR model, which uses an exponential kernel without the normalization factor.

Simulations reveal that:

- The NCF-SIQR model, through kernel normalization, can shift both the timing and magnitude of the epidemic peaks in the I and Q compartments compared to the unnormalized CF and standard Caputo SIQR models.
- For the same fractional order $\alpha < 1$, the NCF kernel leads to epidemic curves that may exhibit earlier or delayed peaks, depending on parameters, highlighting the importance of normalization.
- At very low values of α, all fractional SIQR models retain pronounced memory effects, but the normalization in the NCF approach guarantees that the total memory weight sums to one, which can make the resulting dynamics more interpretable and physically realistic.

Overall, the NCF-SIQR numerical method effectively incorporates memory effects using a normalized kernel. Proper choice of time step, validation against the classical SIQR model, and direct comparison to standard Caputo and CF results provide insight into the influence of memory normalization on epidemic dynamics in quarantine-type compartmental models.

7. Numerical simulations and discussion

To comprehensively investigate the impact of memory effects and kernel normalization in epidemic modeling, we conducted a series of numerical experiments using the NCF fractional SIQR model. All simulations employ the discretization scheme detailed in Section 6, with model parameters and initial conditions reflecting realistic epidemic scenarios.

Unless otherwise specified, the infection rate was set to $\beta = 0.4$, the recovery rate from the infectious class to $\gamma = 0.15$, the isolation rate to $\delta = 0.1$, and the recovery rate from quarantine to $\eta = 0.05$. The initial population fractions were chosen as $S(0) = 0.97$, $I(0) = 0.01$, $Q(0) = 0.01$, and $R(0) = 0.01$, and the final simulation time was $T = 20$ days with a time step $h = 0.05$. The primary focus was on fractional orders $\alpha = 0.95, 0.80, 0.75$, representing a transition from nearly classical dynamics to regimes dominated by memory effects.

Figures 2–6 present the compartmental evolution of the classical SIQR model compared to the fractional NCF-SIQR model at various values of α. For the integer-order model (Figure 2), the

infectious population exhibits a sharp early peak, while the quarantined class rises correspondingly. By contrast, in the NCF-SIQR model (Figures 3–6), decreasing the fractional order α delays and flattens the epidemic peak. Stronger memory effects (smaller α) cause the epidemic to progress more gradually, resulting in reduced peak infectious and quarantined populations.

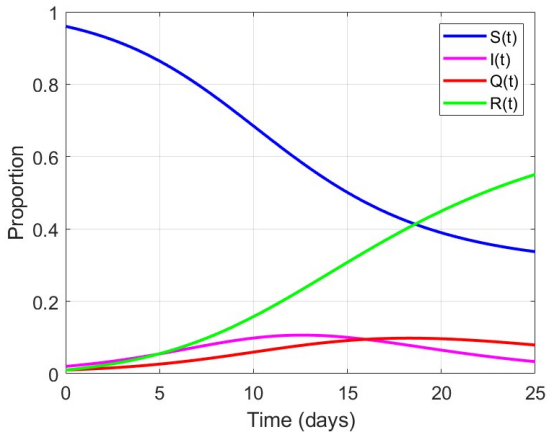

Figure 2. The Classical SIQR Model 3.1.

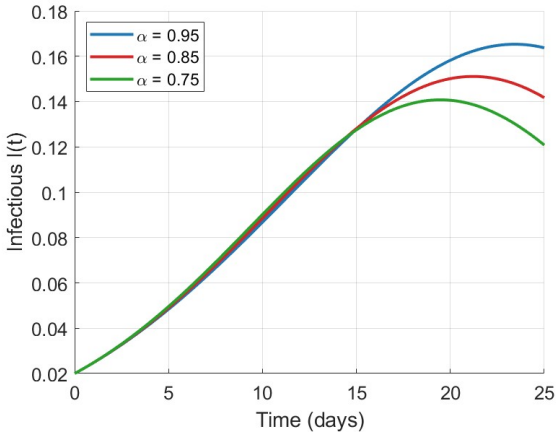

Figure 3. The Infectious population for different values of α.

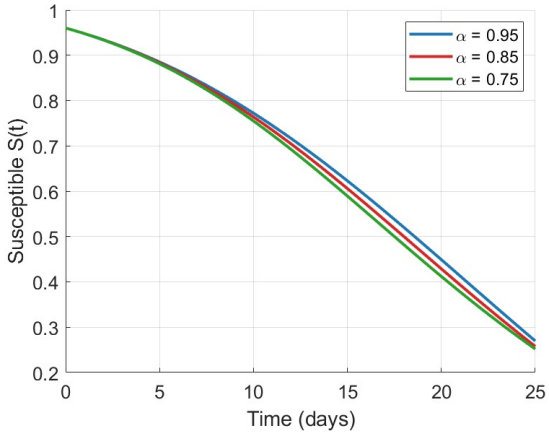

Figure 4. The Susceptible population for different values of α.

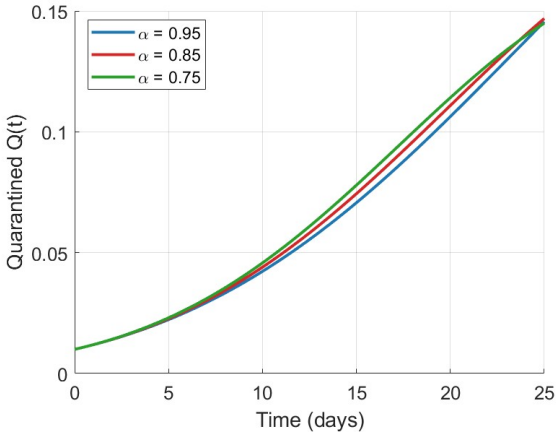

Figure 5. The Quarantined population for different values of α.

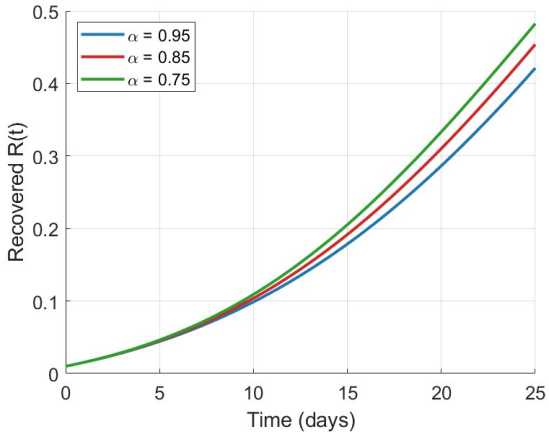

Figure 6. The Recovered for different values of α.

Figures 7–10 illustrate the influence of both memory and infection rate. Surface plots of peak

values $I_{\max}$, $Q_{\max}$, $S_{\min}$, and $R_{\max}$ as functions of α and β reveal that higher memory (lower α) and smaller infection rates consistently yield less severe outbreaks. In contrast, large α and high β values recover the classical epidemic dynamics with rapid transitions and higher peaks in the infectious and quarantined classes.

Figures 11–14 examine the sensitivity of epidemic outcomes to varying initial proportions of infectious (I_0), susceptible (S_0), quarantined (Q_0), and recovered (R_0) individuals. While early-stage epidemic trajectories are shifted by these variations, the long-term qualitative behavior is primarily governed by the memory parameter α and the epidemiological rates $(\beta, \gamma, \delta, \eta)$. This indicates that memory effects dominate initial-condition sensitivity, offering more robust predictions under parameter uncertainty.

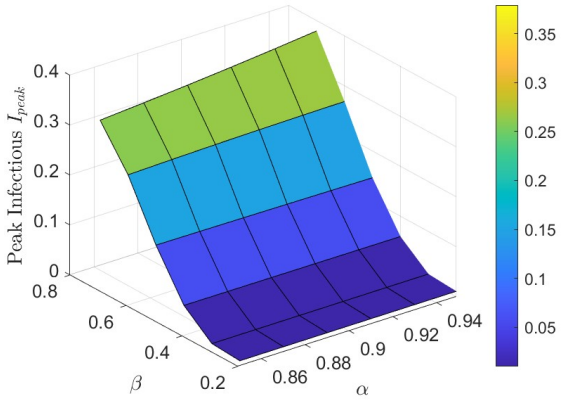

Figure 7. Peak infectious cases I_{peak} as a function of fractional order α and infection rate β.

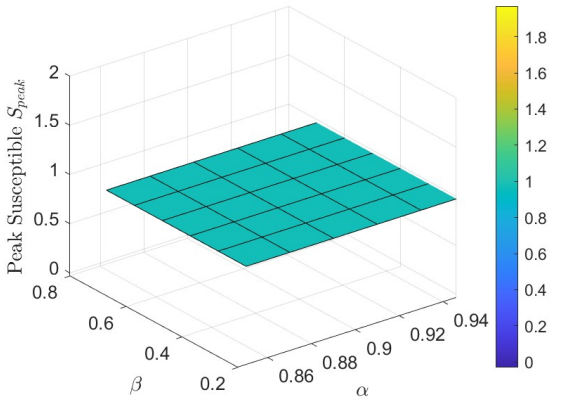

Figure 8. Peak Susceptible cases S_{peak} as a function of fractional order α and infection rate β.

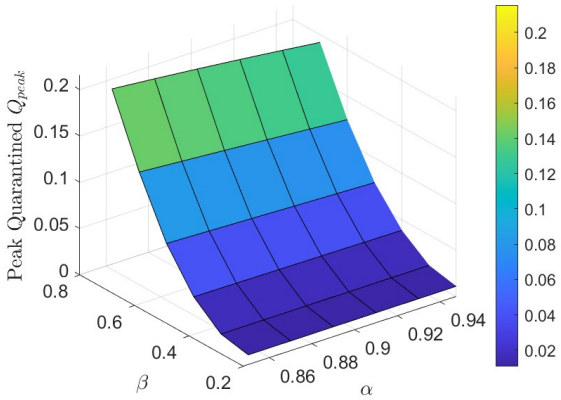

Figure 9. Peak Quaeantined cases Q_{peak} as a function of fractional order α and infection rate β.

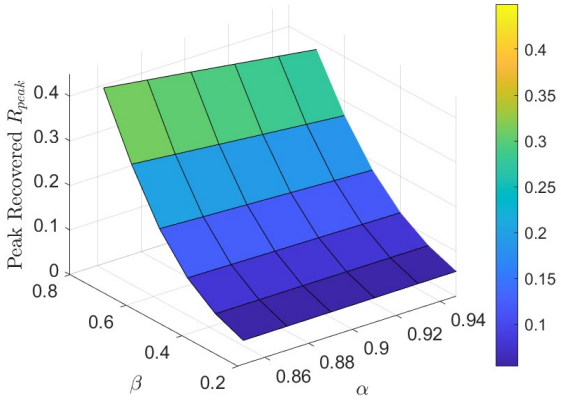

Figure 10. Peak recovered cases R_{peak} as a function of fractional order α and infection rate β.

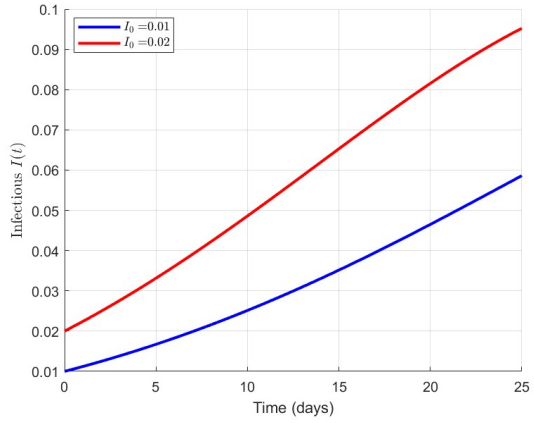

Figure 11. Effect of varying initial infectious proportion I_0 on the time evolution of infectious cases I(t).

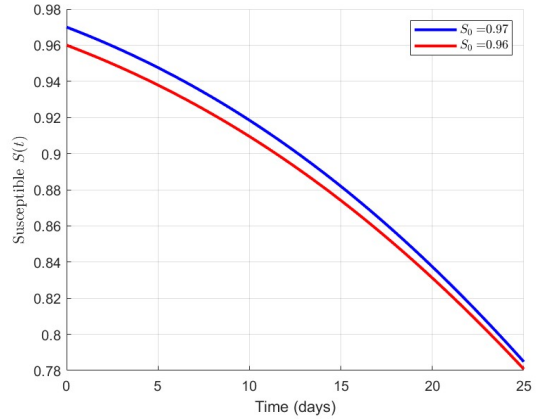

Figure 12. Effect of varying initial susceptible proportion S_0 on the time evolution of susceptible cases S(t).

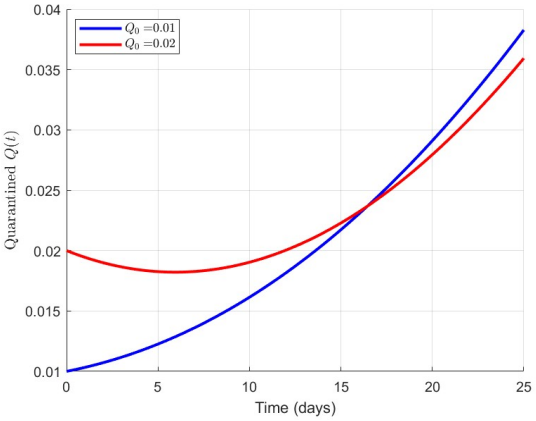

Figure 13. Effect of varying initial quarantined proportion Q_0 on the time evolution of recovered cases Q(t).

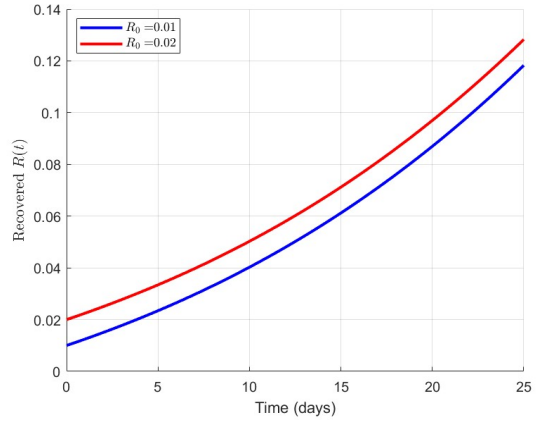

Figure 14. Effect of varying initial recovered proportion R_0 on the time evolution of recovered cases R(t).

The simulations confirm that the NCF derivative substantially modifies epidemic dynamics compared to classical and unnormalized fractional SIQR models. Normalization ensures a consistent weighting of historical states, yielding more interpretable and physically realistic predictions. Importantly, quarantine efficacy is magnified under strong memory regimes, as delayed epidemic peaks provide more time for intervention strategies to take effect. The NCF-SIQR model thus provides a flexible and powerful framework for exploring the interplay between memory, quarantine, and disease progression, with valuable implications for both theoretical analysis and public health forecasting.

To validate the proposed numerical scheme, an ANN was designed and implemented to approximate the compartmental solutions of the NCF-SIQR model. The dataset used for ANN training was generated entirely from high-precision numerical simulations based on the fractional Adams–Bashforth method. The generated data were systematically divided into three non-overlapping subsets: 70% for training, 15% for testing, and 15% for validation. This split ensures that the network is trained on a sufficiently large dataset, while retaining independent subsets for unbiased evaluation of generalization capability. Each subset was analyzed under distinct fractional-order settings to examine the ANN's ability to handle variations in the memory parameter α.

For formalization, we define the ANN mapping as

$$\mathcal{F} : X \longrightarrow Y,$$

where X denotes the input space (e.g., discrete time points t_n) and Y represents the corresponding approximated solution values for the SIQR compartments (S, I, Q, R). The training objective is to minimize the Mean Squared Error (MSE) loss function:

$$\text{MSE} = \frac{1}{n}\sum_{i=1}^{n}(y_i - \hat{y}_i)^2,$$

where y_i are the reference values obtained from the numerical scheme and $\hat{y}_i$ are the predicted outputs from the ANN.

The chosen network architecture is a fully connected feedforward neural network consisting of one input layer, two hidden layers with 10 neurons each, and one output layer. Nonlinear sigmoid activation functions are applied in the hidden layers to capture complex dynamics, while a linear activation function is used in the output layer to preserve the continuous range of model solutions. The selection of this relatively compact architecture is based on the trade-off between representational capacity and computational efficiency.

The network is trained using the Levenberg-Marquardt optimization algorithm with backpropagation, a learning rate of 0.01, and a maximum of 1000 epochs. To prevent overfitting, early stopping is employed: the training process halts if the validation loss does not improve over 10 consecutive epochs. Initial network weights are assigned using the Nguyen–Widrow initialization method to accelerate convergence and improve the starting point for optimization. Training is performed in `MATLAB R2024a` on a workstation equipped with an Intel Core i7 processor and 16 GB RAM, ensuring reproducibility and efficient execution.

The purpose of the ANN in this work is solely as a high-fidelity solution approximator, reproducing the temporal dynamics of the NCF-SIQR model obtained from numerical simulations. It is not intended for parameter estimation or direct prediction from empirical epidemiological datasets. This controlled

setting allows for the direct assessment of how well the ANN can replicate solutions governed by fractional-order memory effects.

The theoretical foundation for employing such a network lies in the universal approximation theorem, which guarantees that a feedforward network with at least one hidden layer can approximate any continuous function on a compact domain, provided that there are sufficient neurons and appropriate activation functions. In this context, the ANN is expected to learn the mapping between time and compartment values for different fractional orders, effectively capturing both smooth and rapidly varying solution profiles.

Performance evaluation is conducted using multiple metrics, including the final MSE, regression plots comparing predicted and reference values, and error distribution histograms. Low MSE values, regression lines closely aligned with the 45° reference line, and tightly clustered error distributions confirm that the ANN successfully replicates the numerical solution trajectories of the NCF-SIQR model across different memory regimes. The statistical results demonstrate the robustness, consistency, and accuracy of the ANN-based solution approximation approach.

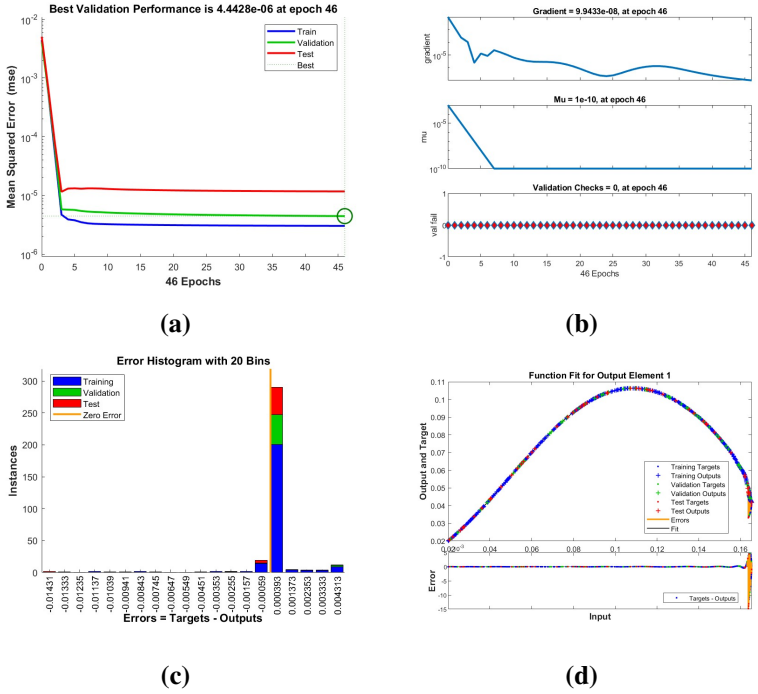

Figure 15. Statistical performance of the proposed model is illustrated through: (a) mean squared error, (b) regression outcomes, (c) error distribution histogram, and (d) ANN training performance.

Figure 15(a) illustrates the model's performance at the 46 epoch, where an MSE of approximately 4.4428e-06 was achieved. The training progression is shown in Figure 15(b), while Figure 15(c) presents the error histogram, indicating a minimum value of 0.000393 as the most accurate outcome observed in this experiment. Figure 15(d) demonstrates both the prediction errors and the best fit for the training and testing datasets. Additionally, Figure 16 displays the regression analysis applied to the complete dataset, which includes both the training and testing sets. The close alignment of the data points with the regression line confirms the model's strong training performance. The coefficient of

determination R is approximately equal to 1.

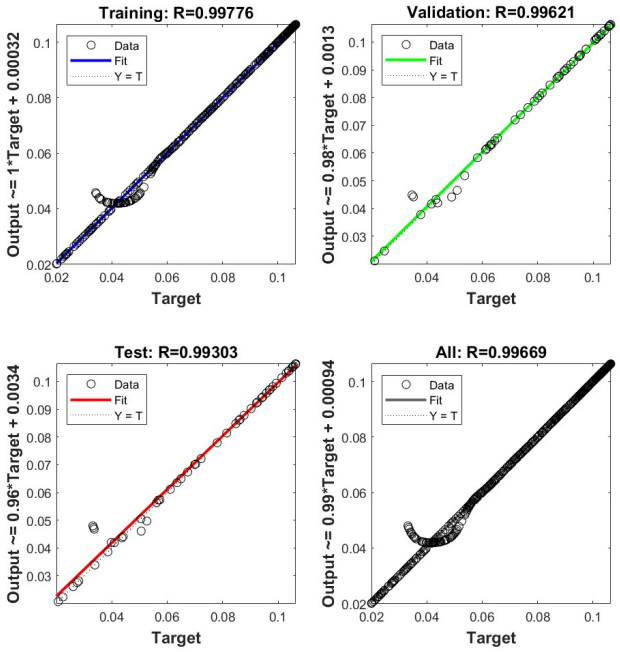

Figure 16. Dynamic visualization of regression results using ANNs applied to the proposed system.

Figure 17(a) presents the model's performance at the 37 epoch, with a reported MSE of 1.5705e-09. Training progression is displayed in Figures 17(b) and 17(c). The error distribution is shown in Figure 17(d), where the minimum value recorded in this experiment is 4.2e-06. Figure 17(d) also illustrates the best alignment between the model predictions and the actual values for both training and testing datasets, along with their respective errors. The regression outcomes for the training, testing, and overall data are summarized in Figure 18. The concentration of data points along the regression line confirms that the ANN was trained successfully. The correlation coefficient R obtained is 1.

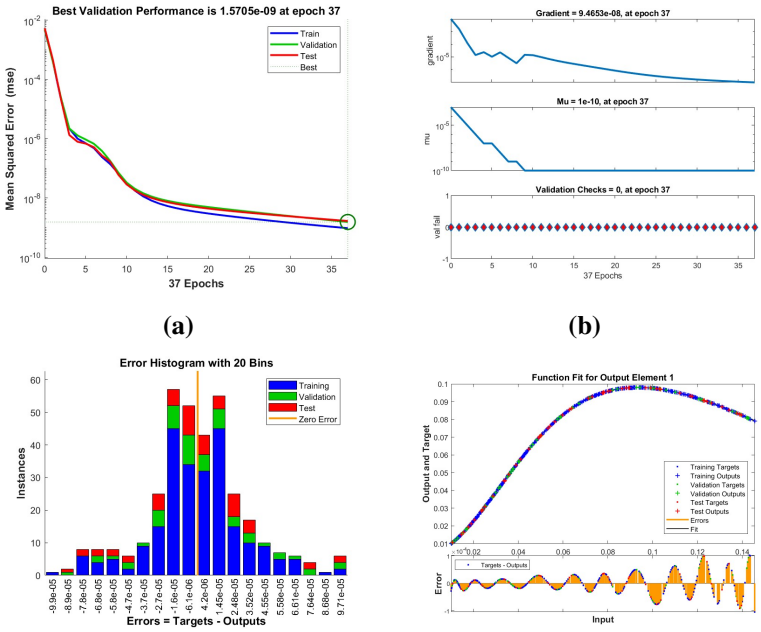

Figure 17. Statistical performance of the proposed model is illustrated through: (a) mean squared error, (b) regression outcomes, (c) error distribution histogram, and (d) ANN training performance.

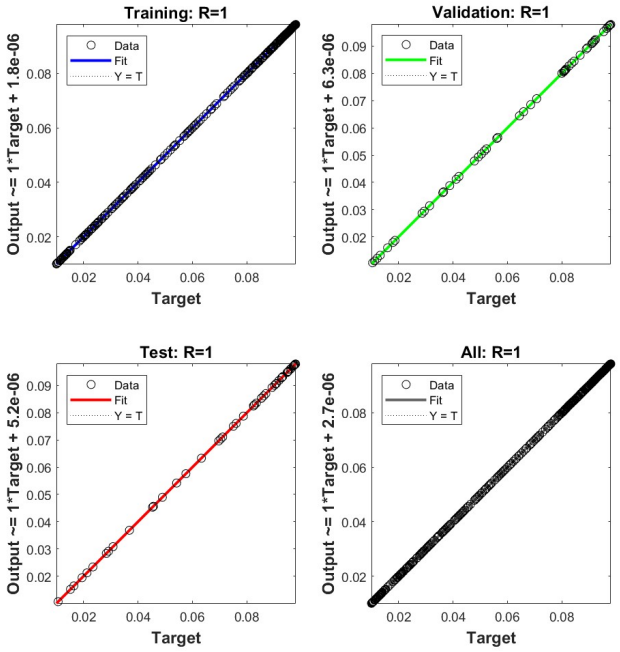

Figure 18. Dynamic visualization of regression results using ANNs applied to the proposed system.

Figure 19(a) presents the model's accuracy at epoch 104, yielding an MSE of approximately 1.9118e-13. The progression of the training phase is depicted in Figures 19(b) and 19(c). The error histogram, shown in Figure 19(c), reveals a minimum error value of -8.6e-09. Figure 19(d) demonstrates the best fit between the predicted and actual data for both training and testing, alongside their corresponding errors. Additionally, the regression analysis for the complete dataset is presented in Figure 20. The precise alignment of the data points along the regression line indicates that the neural network was trained effectively. The resulting correlation coefficient R is approximately equal to 1.

Figure 21(a) illustrates the model's performance at the 101 epoch, yielding an MSE of approximately 5.2028e-13. The training dynamics are presented in Figure 21(b), while the error distribution is depicted in Figure 21(c), where the minimum error recorded is 1.04e-08. Figure 21(d) shows the best alignment between predicted and actual data for both training and testing sets, along with corresponding error measurements. The regression analysis, covering all phases of training and testing, is displayed in Figure 22. The precise alignment of data points along the regression line confirms that the ANN has been trained effectively. The correlation coefficient R obtained is approximately 1.

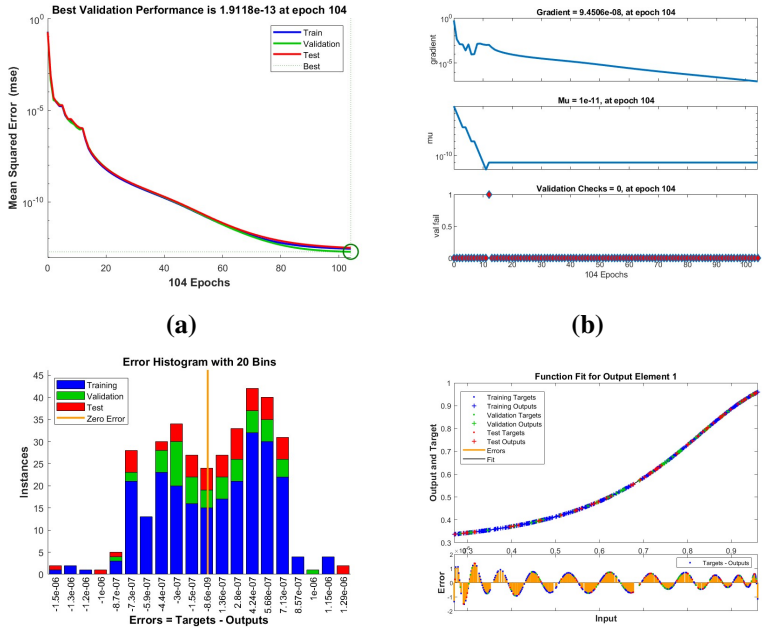

Figure 19. Statistical performance of the proposed model is illustrated through: (a) mean squared error, (b) regression outcomes, (c) error distribution histogram, and (d) ANN training performance.

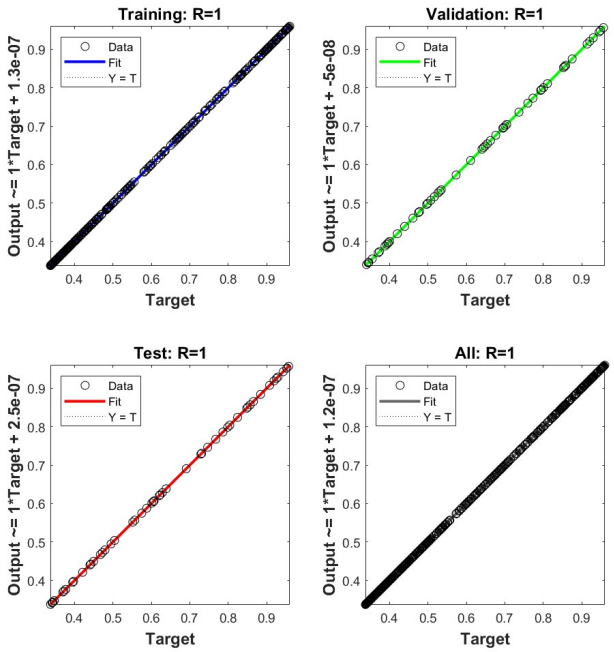

Figure 20. Dynamic visualization of regression results using ANNs applied to the proposed system.

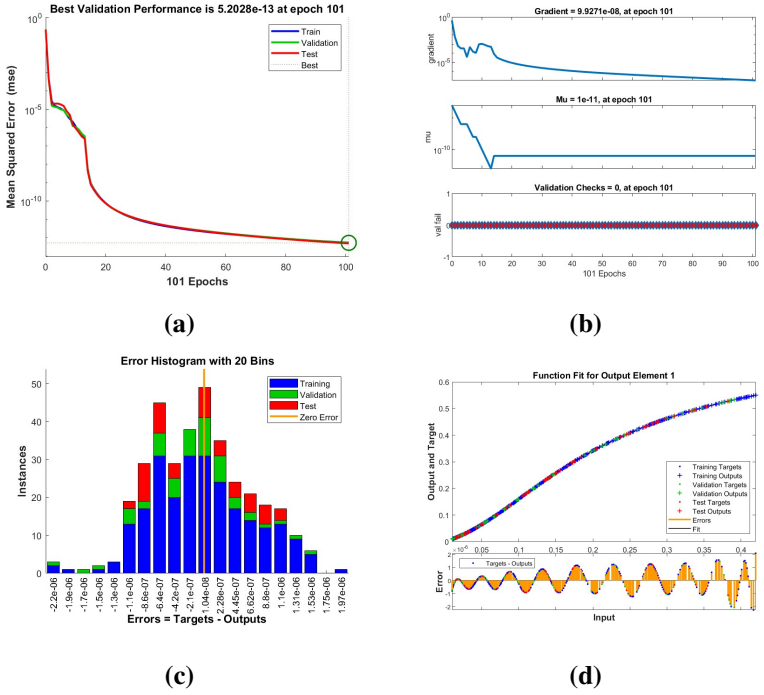

Figure 21. Statistical performance of the proposed model is illustrated through: (a) mean squared error, (b) regression outcomes, (c) error distribution histogram, and (d) ANN training performance.

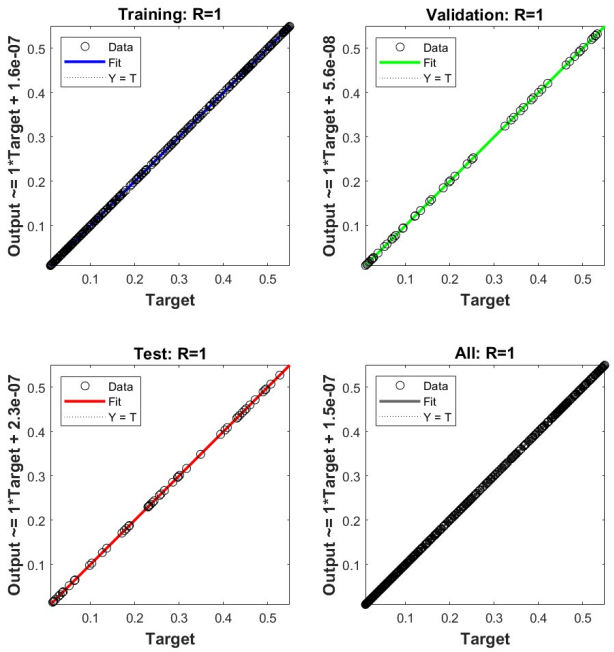

Figure 22. Dynamic visualization of regression results using ANNs applied to the proposed system.

7.1. Linking machine learning applications and the S.A.F.E. framework

To enhance the real-world relevance and AI alignment of this work, we emphasize that the application of ANNs to the fractional SIQR model extends beyond merely approximating solutions. In contemporary epidemic forecasting, machine learning approaches—such as ANNs, LSTM, and GRU architectures have been widely used to predict infection curves, estimate unknown parameters from incomplete data, and support decision-making under uncertainty. Reinforcement learning has also been employed to optimize intervention strategies. These applications demonstrate the growing role of AI in shaping epidemiological modeling and public health responses.

Furthermore, the methodology presented in this paper aligns with the S.A.F.E. machine learning framework, which promotes the development of models that are Secure, Accountable, Fair, and Explainable. In terms of security, the ANN models in this study are trained exclusively on synthetic simulation data, thereby avoiding privacy risks and minimizing the potential for data misuse. Accountability is ensured through a thoroughly documented modeling pipeline, including the specification of training procedures, neural architecture, and performance metrics such as mean squared error and regression outcomes, which enable reproducibility and auditability. The fairness component is addressed through the use of unbiased, deterministic datasets, although the approach's structure permits the future integration of real-world data while enabling fairness monitoring across compartments, such as the infectious, quarantined, and recovered populations. Finally, explainability is incorporated through the use of visual diagnostics, including error histograms, regression plots, and performance trajectories. While the current ANN implementation primarily functions as a solution approximator, future extensions may incorporate interpretability tools, such as SHAP values

or attention mechanisms, to better understand the model's internal reasoning.

By embedding these S.A.F.E. principles into both the design and evaluation of the machine learning component, this work contributes to the development of transparent and trustworthy AI systems in the context of epidemic modeling, supporting the broader movement toward responsible artificial intelligence in health research.

8. Conclusions

This study developed and rigorously analyzed a fractional-order SIQR epidemic model using the NCF derivative, establishing key theoretical results such as existence, uniqueness, positivity, and boundedness to ensure the model's mathematical validity. The proposed numerical scheme effectively captured the influence of memory effects and kernel normalization, with comparative simulations highlighting clear differences between the NCF-SIQR model and its classical and unnormalized fractional counterparts. Coupling the model with ANNs enabled accurate approximation of compartmental solutions, thereby validating the robustness of the numerical method. The results demonstrate that both quarantine efficacy and fractional memory effects play a critical role in shaping epidemic dynamics, reducing peak infectious cases and accelerating recovery under suitable conditions. Looking ahead, potential extensions of this work include applying the NCF-SIQR model to real epidemic datasets for parameter estimation and predictive forecasting, integrating optimal control theory to design effective intervention strategies, and expanding the model to more complex compartmental structures such as SEIQR, vaccination, asymptomatic carriers, or demographic effects. Additional future directions involve incorporating network-based or spatially heterogeneous formulations for multi-region epidemic spread, coupling the framework with uncertainty quantification and Bayesian inference to facilitate robust decision-making under incomplete or noisy data, and exploring advanced machine learning architectures, such as LSTM, GRU, and transformer-based models, to enhance predictive accuracy and interpretability. By combining rigorous fractional-order modeling with machine learning techniques, the proposed framework presents a promising approach for enhancing epidemic forecasting and facilitating the development of effective, evidence-based public health interventions.

Author contributions

Ramsha Shafqat: conceptualization, methodology, formal analysis, investigation, resources, writing-original draft, writing-review & editing, supervision; Ateq Alsaadi: software, investigation, resources, project administration, funding. All authors have read and approved the final version of the manuscript for publication.

Use of Generative-AI tools declaration

The authors declare they have not used Artificial Intelligence (AI) tools in the creation of this article.

Acknowledgments

The authors express their sincere appreciation to Taif University, Saudi Arabia, for the support it has offered under project number (TU-DSPP-2024-259).

Conflict of interest

All authors declare no conflicts of interest in this paper.

References

1. H. W. Hethcote, The mathematics of infectious diseases, *SIAM Rev.*, **42** (2000), 599–653. https://doi.org/10.1137/S0036144500371907
2. F. Brauer, Mathematical epidemiology: past, present, and future, *Infectious Disease Modelling*, **2** (2017), 113–127. https://doi.org/10.1016/j.idm.2017.02.001
3. W. O. Kermack, A. G. McKendrick, A contribution to the mathematical theory of epidemics, *Proc. R. Soc. Lond. A*, **115** (1927), 700–721. https://doi.org/10.1098/rspa.1927.0118
4. K. Diethelm, An investigation of some nonclassical methods for the numerical approximation of Caputo-type fractional derivatives, *Numer. Algor.*, **47** (2008), 361–390. https://doi.org/10.1007/s11075-008-9193-8
5. R. Shafqat, A. Alsaadi, Artificial neural networks for stability analysis and simulation of delayed rabies spread models, *AIMS Mathematics*, **9** (2024), 33495–33531. https://doi.org/10.3934/math.20241599
6. H. G. Sun, A. L. Chang, Y. Zhang, W. Chen, A review on variable-order fractional differential equations: mathematical foundations, physical models, numerical methods and applications, *Fract. Calc. Appl. Anal.*, **22** (2019), 27–59. https://doi.org/10.1515/fca-2019-0003
7. A. Turab, R. Shafqat, S. Muhammad, M. Shuaib, M. F. Khan, M. Kamal, Predictive modeling of hepatitis B viral dynamics: A caputo derivative-based approach using artificial neural networks, *Sci. Rep.*, **14** (2024), 21853. https://doi.org/10.1038/s41598-024-70788-7
8. R. Shafqat, A. Ateq, A. Alubaidi, A fractional-order alcoholism model incorporating hypothetical social influence: A theoretical and numerical study, *J. Math.*, **2025** (2025), 6773909. https://doi.org/10.1155/jom/6773909
9. A. Atangana, D. Baleanu, New fractional derivatives with nonlocal and non-singular kernel: theory and application to heat transfer model, (2016), arXiv:1602.03408. https://doi.org/10.48550/arXiv.1602.03408
10. N. Sene, SIR epidemic model with Mittag–Leffler fractional derivative, *Chaos Soliton. Fract.*, **137** (2020), 109833. https://doi.org/10.1016/j.chaos.2020.109833
11. J. Kim, A normalized Caputo–Fabrizio fractional diffusion equation, *AIMS Mathematics*, **10** (2025), 6195–6208. https://doi.org/10.3934/math.2025282

12. J. Zhang, D. S. Yang, H. G. Zhang, Y. C. Wang, B. W. Zhou, Dynamic event-based tracking control of boiler turbine systems with guaranteed performance, *IEEE T. Autom. Sci. Eng.*, **21** (2024), 4272–4282. https://doi.org/10.1109/TASE.2023.3294187

13. J. L. You, Z. Q. Zhang, Finite-time synchronization of fractional order chaotic systems by applying the maximum-valued method of functions of five variables, *AIMS Mathematics*, **10** (2025), 7238–7255. https://doi.org/10.3934/math.2025331

14. Y. G. Kao, C. H. Wang, H. W. Xia, Y. Cao, Projective synchronization for uncertain fractional reaction-diffusion systems via adaptive sliding mode control based on finite-time scheme, In: *Analysis and control for fractional-order systems*, Singapore: Springer, 2024, 141–163. https://doi.org/10.1007/978-981-99-6054-5_8

15. Y. G. Kao, Y. Li, J. H. Park, X. Y. Chen, Mittag–Leffler synchronization of delayed fractional memristor neural networks via adaptive control, *IEEE T. Neur. Net. Lear.*, **32** (2021), 2279–2284. https://doi.org/10.1109/TNNLS.2020.2995718

16. Y. Cao, Y. G. Kao, J. H. Park, H. B. Bao, Global Mittag–Leffler stability of the delayed fractional-coupled reaction-diffusion system on networks without strong connectedness, *IEEE T. Neur. Net. Lear.*, **33** (2022), 6473–6483. https://doi.org/10.1109/TNNLS.2021.3080830

17. Y. Cao, Y. G. Kao, Z. Wang, X. S. Yang, J. H. Park, W. Xie, Sliding mode control for uncertain fractional-order reaction-diffusion memristor neural networks with time delays, *Neural Networks*, **178** (2024), 106402. https://doi.org/10.1016/j.neunet.2024.106402

18. Y. G. Kao, Y. Cao, X. Y. Chen, Global Mittag-Leffler synchronization of coupled delayed fractional reaction-diffusion Cohen–Grossberg neural networks via sliding mode control, *Chaos*, **32** (2022), 113123. https://doi.org/10.1063/5.0102787

19. I. Goodfellow, Y. Bengio, A. Courville, *Deep learning*, Cambridge: MIT Press, 2016.

20. S. Haykin, *Neural networks: a comprehensive foundation*, New Jersey: Prentice Hall PTR, 1994.

21. Z. F. Yang, Z. Q. Zeng, K. Wang, S.-S. Wong, W. H. Liang, M. Zanin, et al, Modified SEIR and AI prediction of the epidemics trend of COVID-19 in China under public health interventions, *J. Thorac. Dis.*, **12** (2020), 165–174. https://doi.org/10.21037/jtd.2020.02.64

22. M. Caputo, M. Fabrizio, A new definition of fractional derivative without singular kernel, *Progr. Fract. Differ. Appl.*, **1** (2015), 73–85.

23. M. Jornet, Theory on new fractional operators using normalization and probability tools, *Fractal Fract.*, **8** (2024), 665. https://doi.org/10.3390/fractalfract8110665

24. M. Caputo, Linear models of dissipation whose Q is almost frequency independent-II, *Geophysical Journal of the Royal Astronomical Society*, **13** (1967), 529–539. https://doi.org/10.1111/j.1365-246X.1967.tb02303.x

AIMS Press